JOURNAL OF MATERIALS SCIENCE 21 (1986) 4281–4288

# Dynamic crack propagation behaviour of rubber-toughened poly(methyl methacrylate)

J. MILIOS, G. C. PAPANICOLAOU
*Department of Theoretical and Applied Mechanics, The National Technical University of Athens, 15773 Athens, Greece*

R. J. YOUNG*
*Department of Materials, Queen Mary College, London E1 4NS, UK*

Dynamic crack propagation has been studied in detail for a series of transparent rubber-toughened samples of poly(methyl methacrylate) using a combination of high-speed photography and the optical method of transmitted caustics. The dynamic stress intensity factor has been measured as a function of rubber content, crack length and loading rate. The dynamic stress intensity factor is found to increase significantly as the rubber content increases, which is consistent with the improvement in impact behaviour found on the addition of rubber particles. It is proposed that the toughening takes place through crack tip blunting caused by localized shear yielding induced by the presence of the rubber particles.

## 1. Introduction

Significant improvements in the mechanical properties of brittle polymers can be achieved by the incorporation of second-phase particles which can be either rigid [1–3] or rubbery [4, 5]. Because of this there has been an increasing interest over recent years in the study of the crack propagation behaviour in such multiphase polymeric particulate composites. It is found that a large number of factors can influence crack propagation behaviour. These factors include:

(a) the size and distribution of particles [4, 6],
(b) the mechanical properties of the particles and matrix [1, 7],
(c) the volume fraction of particles [1, 3, 7],
(d) the rate and temperature of testing [3, 8], and
(e) the strength of interfacial bonding [9].

Second-phase particles are often added to brittle polymers to improve their performance under impact loading. This has led to a number of studies of the impact fracture of such "toughened" polymers [4, 5, 10]. However, fracture under dynamic loading conditions can also be studied in detail using a combination of high-speed photography to measure crack velocity $\dot{a}$ and determination of dynamic stress intensity factors $K_I^d$ using the method of caustics [11–16]. This has enabled correlations to be made between $K_I^d$ and $\dot{a}$ [12–14] and allowed the crack propagation behaviour to be followed in detail.

Although most dynamic crack propagation studies have been confined to single-phase transparent polymers such as poly (methyl methacrylate) (PMMA) and epoxy resins, dynamic crack propagation has also been investigated in certain multiphase systems [15, 16]. For example, it has been demonstrated that for a crack propagating through bimaterial plates when the crack propagates from a ductile material to a brittle one there is an increase in crack propagation velocity, while the opposite behaviour is observed for a crack going from a brittle material to a more ductile phase [15, 16].

Dynamic crack propagation has also been followed as a function of volume fraction in epoxy resins filled with iron particles [7]. It was found that the mean crack propagation velocity decreased linearly with increasing filler volume fraction, while the presence of filler particles in the epoxy matrix resulted in bifurcation or multiple splitting of the cracks accompanied by a reduction in the critical crack propagation velocity with increasing filler volume fraction.

It is well established that the strength of the interfacial bond is important in controlling the mechanical behaviour of multiphase polymer composites. Epoxy resin bimaterial plates with various levels of bonding at the interface [18, 19] have been used to model interfacial effects during dynamic crack propagation in composites. It has been demonstrated that a crack propagating through one of the plates at a constant velocity decelerates as it reaches a short distance from the interface, and then stops for a few microseconds before entering the second phase. If the bonding at the interface is weak a crack is found to propagate along the interface in two branches, due to the increased shear stress at the interface, before it enters the second phase as two cracks [18, 19].

The highest levels of toughening in glassy polymers are generally achieved by the addition of second-phase rubbery particles [1, 4]. However, such materials are generally opaque making dynamic crack propagation studies rather difficult. Over recent years, certain grades of toughened "impact-modified" acrylic polymers have become available in which the transparency

*Present address*: Department of Polymer Science and Technology, UMIST, PO Box 88, Manchester M60 1QD, UK.

0022–2461/86 $03.00 + .12 

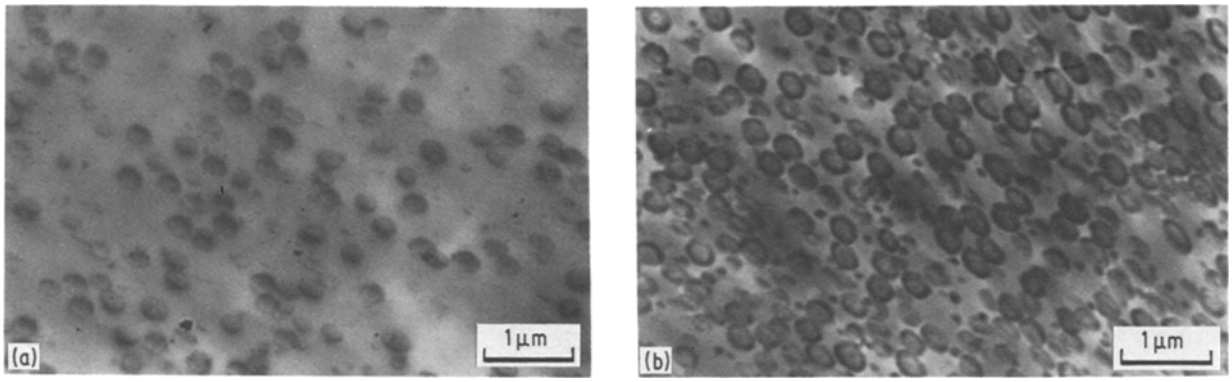


*Figure 1* Transmission electron micrographs of sections of the rubber-modified PMMA samples containing (a) 10 and (b) 40 vol % of particles.

has been maintained. This is done by matching the refractive indices of the rubber particles and the poly (methyl methacrylate) (PMMA) matrix and reducing the size of the particles to below the wavelength of light [4, 5]. In this present investigation, dynamic crack propagation in a series of transparent toughened acylic polymers containing different volume fractions of rubber particles has been followed using a combination of high-speed photography and the method of transmitted optical caustics. This has enabled a detailed study to be made of the variation of the dynamic stress intensity factor, $K_I^d$, with particle volume fraction, crack length and loading rate.

## 2. Materials

The materials used in this present study were a series of injection-moulded Oroglas acrylic polymers supplied by Rohm and Haas (UK) Ltd. They included V811, a medium molar mass, medium flow injection moulding grade of poly(methyl methacrylate), and three other rubber-toughened grades of PMMA containing approximately 10, 20 and 40% volume fractions ($V_p$) of similar rubber particles. The compositions of the rubber-toughened grades were confirmed by dissolving the PMMA matrix in acetone, centrifuging and weighing the insoluble fraction. The structure of the three rubber-toughened polymers was examined using transmission electron microscopy. Sections $\sim 0.2\,\mu m$ thick were obtained using a glass-knived ultramicrotome and they were examined, without staining, in a Jeol 100CX transmission electron microscope operated at 100 kV. Fig. 1 shows electron micrographs of sections of the 10% and 40% grades, and it can be seen that the structures contain particles of the order of $0.3\,\mu m$ in size. The particles are spherical but appear in the micrographs to be slightly oval due to distortion during sectioning. It is difficult to determine the exact volume fractions of the particles from these sections because their exact thickness is not known. However, it can be seen that the highest particle volume fraction material contains by far the largest number of particles.

An important point to note is that particles are not homogeneous but have a dark ring around their outside. It appears that they may be multi-stage particles produced by sequential emulsion polymerization [20]. For example, three-stage particles consist of a rigid polymer core surrounded by a rubbery shell of butyl acrylate/styrene copolymer rubber, and an outer shell of PMMA. Graft-linking can be used to give good interfacial cohesion between the different layers and the core is often cross-linked to reduce particle breakdown during processing [5]. When the particles are incorporated into a PMMA matrix the outer shell of the particles becomes part of the matrix, and so the structure appears in electron micrographs such as in Fig. 1 as consisting of rubber particles with a solid core. The rubber appears as a dark shell in the micrographs even though the sections are not stained, although it is not clear how the contrast arises.

## 3. The optical method of transmitted caustics

The optical method of transmitted caustics was used for the determination of the stress intensity factor at the tip of the propagating cracks and the crack propagating velocities. According to this method, a convergent or divergent light beam impinges on the specimen in the vicinity of the crack tip and the transmitted rays are collected at a reference plane parallel to the plane of the specimen. The stress concentration in the vicinity of the crack tip results in a reduction of the thickness of the specimen due to the Poisson's ratio effect and also to a change of the refractive index of the material in this area. In this way, the stress singularity at the crack tip is transformed into an optical singularity in the reference plane by the refraction of light. The deflected rays from the neighbourhood of the crack tip are concentrated along a strongly illuminated curve (caustic) in the reference plane, while the area enveloped by the caustic becomes a shadowed area.

The stress intensity factor at the tip of the crack can be calculated from the geometric characteristics of the caustic with a high degree of accuracy. Further, the position of the extremities of the moving crack front at any instant of time can be accurately deduced from the respective positions of the caustics, and the instantaneous value of the crack propagation velocity can be derived. The stress intensity factor for the specimens used, and for a crack propagating transversely to the applied load, is given [14] by

$$K_I^d = C\left(\frac{D_t^{max}}{\delta_{t(c)}^{max}}\right)^{5/2} \quad (1)$$

where

$$C = \frac{1.671}{z_0 d c_t \lambda_m^{3/2}} \quad (2)$$

and

$$\lambda_m = \frac{z_i}{z_0 + z_i} \quad (3)$$

$\lambda_m$ denotes the magnification ratio of the optical set-up, $z_0$ the distance between the specimen and the reference screen, $z_i$ the distance between the reference plane and the focus of the light beam, $d$ the thickness of the specimen, $c_t$ the stress optical coefficient, $D_t^{max}$ the transverse diameter of the caustic at the reference screen and $\delta_{t(c)}^{max}$ a correction factor for the diameter of the caustic which takes into consideration the dynamic effect due to crack propagation and which is given in published monographs [7].

## 4. Experimental procedure

A Cranz–Schardin high-speed camera producing 24 sparks with a maximum frequency of $10^6$ frames per second was used for the study of the dynamic crack propagation. The regulation of the spark frequency was made such that spark groups of (4), (5), (5), (5), (5) intervals were produced which enabled observation of the whole process of crack propagation. A Carl-Schenk hydropulse high-speed testing machine was used for the dynamic fracture of the specimens. It has electronic displacement control, a maximum dynamic load of 40 kN and a maximum possible strain rate $\dot{\varepsilon} = 80\,\text{sec}^{-1}$. The applied dynamic load was recorded using a quartz force-transducer.

The synchronization of the fracture process with the high-speed camera was achieved by means of a silver-contact circuit which triggers the sparks on the initiation of crack opening. The set-up also employs a delay circuit which could be activated if crack propagation was not instantaneous.

The optical part of the experimental arrangement contains a concave reflector of 0.5 m diameter and of focal distance $f = 7.00$ m. The light beam emitted from each spark was reflected from the concave mirror, and after passing through the specimen was focused at the respective lens of the Cranz–Schardin camera. The experimental arrangement used in the present study is shown elsewhere [15].

For the present experimental study, eight specimens of each type of material were used, all having dimensions of 100 mm × 25 mm × 3 mm and containing an artificial edge crack 8 mm long. The artificial initial cracks were sawn by means of a fine saw-disc, so that the opening between the adjacent lips of the artificial cracks was less than 0.3 mm. This kind of specimen enables detection of the process of crack initiation and observation of the first stages of crack propagation.

Half of the specimens were fractured at a loading rate producing a strain rate of $12\,\text{sec}^{-1}$ while the rest of the specimens were fractured at a strain rate of $4\,\text{sec}^{-1}$. It was therefore possible to follow the influence of the strain rate on the fracture process in the different materials.

Specimens of the same dimensions with those used in the dynamic fracture experiments were also used as control specimens for the evaluation of Poisson's ratio, $v$. The specimens were loaded in tension in an Instron test machine, while electrical strain gauge sensors were used in the measurements of Poisson's ratio.

An interferometric method was used [17] for the evaluation of the stress optical constant $c_t$ of the materials investigated. Specimens in the form of flat parallel-sided plates of the same dimensions as those used in the fracture tests were used. Each specimen was mounted on an Instron test machine and loaded in tension, while at the same time monochromatic light with a wavelength $\lambda = 632.8$ nm emitted from an He–Ne laser was projected through the specimen. The reflected rays from each of the faces interferes forming fringes on a reference plane placed at a distance from the specimen. The laser light beam was plane polarized so that it could be aligned with one of the principal stress directions by angular rotation of the laser.

Two measurements were executed along the two principal directions at a generic point of the field for a simple tension specimen, and if $N_1$ and $N_2$ are the numbers of fringes counted along the two principal stress directions 1 and 2, when a particular load is applied to the specimen, the optical contains $\alpha^*$ and $\beta^*$ can be evaluated from the following relations [11]:

$$\alpha^* = \frac{N_1}{2d\sigma} \qquad \beta^* = \frac{N_2}{2d\sigma} \quad (4)$$

where $\sigma$ is the applied stress and $d$ the thickness of the specimen.

Then, the stress-optical coefficient $c_t$ may be found according to the formula

$$c_t = \frac{-\lambda(\alpha^* + \beta^*)}{2} + \frac{v}{E} \quad (5)$$

while the coefficient of optical anisotropy, $\xi_t$, is given by

$$\xi_t = \frac{\lambda(\beta^* - \alpha^*)}{2c_t} \quad (6)$$

## 5. Results and Discussion

### 5.1. Material constants

In order to evaluate the stress intensity factors using the method of caustics it was necessary to calculate the Young's moduli ($E$), Poisson's ratios ($v$) and the stress-optical coefficients ($c_t$) for the different materials. The results, given in Table I, show the expected trends since the Young's moduli decrease and the Poisson's ratios and stress-optical coefficients increase as the amount of rubber in the composites is increased. Although these values are strictly only applicable to low-rate tests, as is conventional [15, 16], they were

TABLE I Experimental values of mechanical and optical characteristics for pure PMMA and rubber-modified grades

| Property | $V_p$ (%) | | | |
|---|---|---|---|---|
| | 0 | 10 | 20 | 40 |
| Tensile modulus (GPa) | 3.4 | 2.4 | 2.2 | 1.5 |
| Poisson's ratio | 0.34 | 0.35 | 0.38 | 0.40 |
| Stress-optical coefficient ($Pa^{-1} \times 10^{-10}$) | 0.560 | 0.776 | 0.835 | 1.442 |

TABLE II Initiation values of stress intensity factors and delay times for PMMA and rubber-modified grades measured for the two different strain rates

| Material | $V_p$ (%) | | | | | | | |
|---|---|---|---|---|---|---|---|---|
| | 0 | | 10 | | 20 | | 40 | |
| Strain rate ($sec^{-1}$) | 4 | 12 | 4 | 12 | 4 | 12 | 4 | 12 |
| $K_I^0$ ($MN m^{-3/2}$) | 1.4 | 1.6 | 1.9 | 1.7 | 2.7 | 2.3 | – | 3.5* |
| Delay time ($\mu$sec) | ~0 | ~0 | 200 | 2 | 340 | 4 | 450 | 10 |

*Just before crack initiation. Probably not strictly valid value.

used to calculate the dynamic stress intensity factors for the high-rate tests.

## 5.2. Effect of loading rate on crack initiation

The delay times before crack propagation took place after initial loading and breaking of the silver contact circuit were determined using the high-speed photographic technique and the values are listed in Table II. For the pure PMMA it was not possible within the resolution of the apparatus ($> 0.1\,\mu$sec) to measure any delay, as cracks were found to propagate as soon as the external load was applied and the optical set-up triggered. However, for the rubber-modified polymers, delays of the order of several hundred microseconds were measured for the strain rate of $4\,sec^{-1}$ and a few microseconds for the higher strain rate of $12\,sec^{-1}$.

It can be seen from Table II that there is an increase in the delay times as the rubber content of the particulate composites increases, which is consistent with an increase in ductility in the materials. There is also a large decrease in delay time for each composite as the strain rate is increased, indicating a more brittle type of behaviour. The processes which take place during this initial loading period are shown in Fig. 2 for the sample containing 40% of particles deformed at $4\,sec^{-1}$ seen at 4 and $448\,\mu$sec after the load was applied. The caustic can be seen as a dark circular area and the diameter of the caustic is related directly to $K_I$ (through Equation 1) and so with the energy stored at the crack tip. Although the crack remains stationary the diameter of the caustic increases during the delay period, corresponding to an increase in $K_I$ due to crack tip blunting [1].

## 5.3. Dynamic crack propagation behaviour

Stress intensity factors and crack propagation velocities were determined using the optical method of caustics. Sets of typical photographs obtained during crack propagation are shown in Figs 3 to 6 for the four types of material. The stress intensity factors $K_I$ can be determined from the diameters of the caustics through Equation 1. It can be seen by comparing the early frames of Figs 3 to 6 that the diameters of the caustics, and hence the stress intensity factors at crack initiation, $K_I^0$, increase with an increasing amount of rubber in the polymer. The values of $K_I^0$ for the different materials deformed at the two different rates are listed in Table II. The effect of loading rate upon $K_I^0$ is rather complex, with it increasing with rate for the pure PMMA but decreasing with rate for the composites.

It was pointed out in Section 3 that the optical method of caustics is based on the elastic solution of the singular stress distribution close to the crack tip, and can only therefore be strictly applied to brittle fracture. The behaviour of the PMMA containing 40% of particles is shown in Fig. 6, where distorted caustics can be seen at the tip of the crack both before and during crack propagation. This shows that under the conditions used, the material containing the highest amount of rubber particles was too ductile for valid dynamic stress intensity factors to be determined. Another indication of the ductility of the material was that the crack did not propagate perpendicular to the stressing direction (vertical in Fig. 6) but at an angle of about 83° to this axis. The dynamic fracture behaviour of the samples with the highest volume fraction of particles (40%) determined over a larger range of loading rates, and using different types and lengths of cracks, will be the subject of future investigations and will not be discussed further here.

Figs 7, 8 and 9 give the variation of the dynamic stress intensity factor $K_I^d$ (normalized with respect to $K_I^0$) with crack length for the different materials. It can be seen that in each case $K_I^d/K_I^0$ is generally higher for the lower strain rates. It is also significant that for the two composite samples $K_I^0/K_I^0$ decreases abruptly soon after the crack starts to propagate (Figs 8 and 9). This is reflected in the reduction of the size of the caustics with time in Figs 4 and 5. It is possible to obtain a clear idea of the dynamic propagation behaviour by comparing a delay time in Table II with Figs 7, 8 and 9. In the case of pure PMMA, crack propagation takes

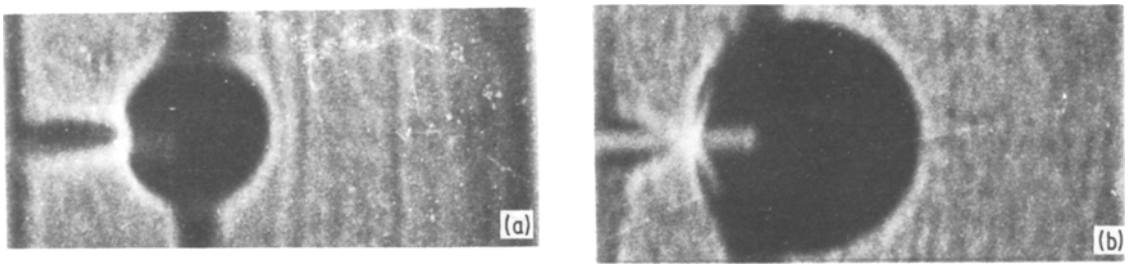


*Figure 2* Photographs of the caustics in the polymer containing 40% of rubber particles obtained at (a) 4 and (b) $448\,\mu$sec prior to crack propagation (strain rate = $4\,sec^{-1}$).

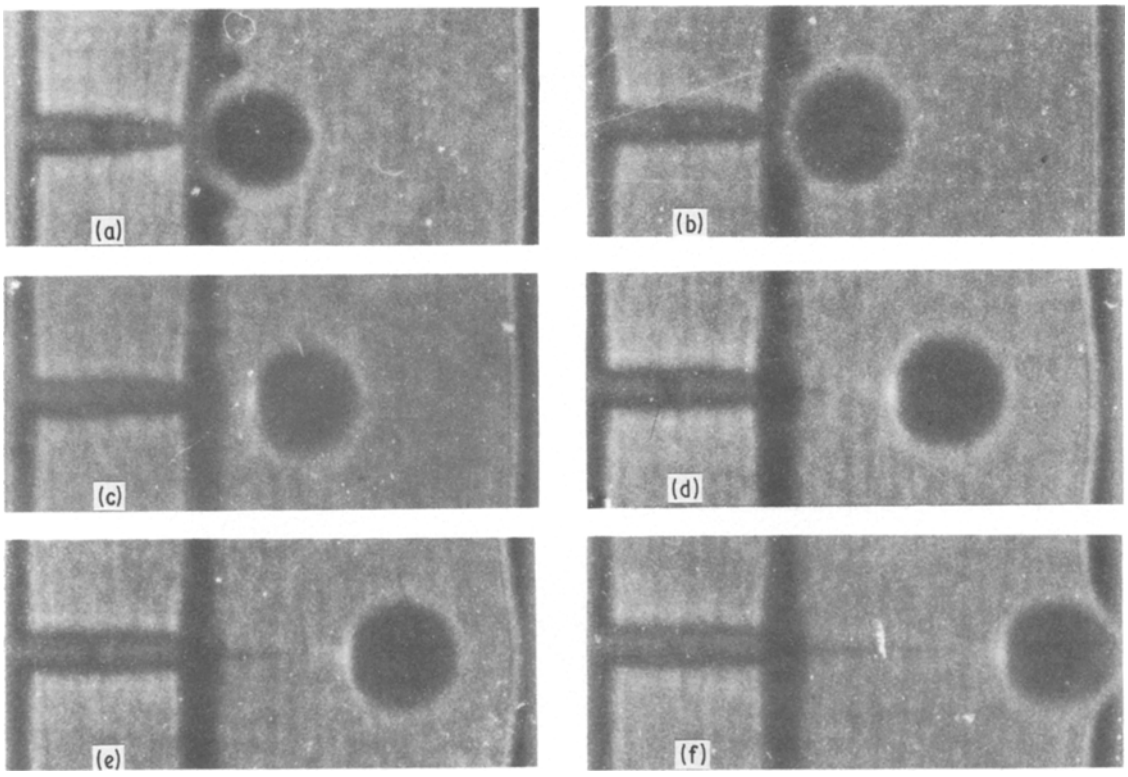


*Figure 3* A series of photographs showing crack propagation in the pure PMMA (strain rate = $4\,sec^{-1}$): (a) 2, (b) 5, (c) 9, (d) 17, (e) 21, (f) 25 $\mu$sec.

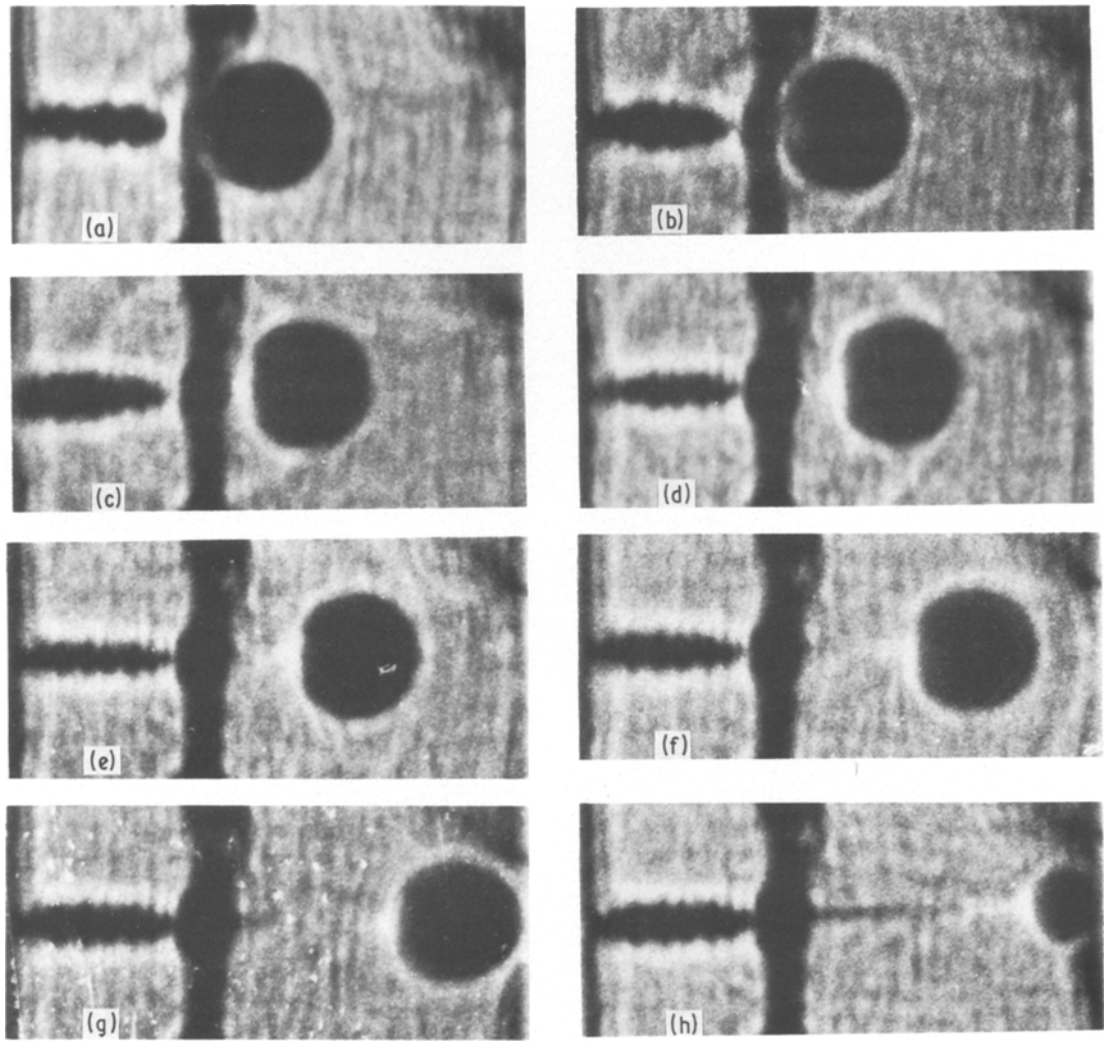


*Figure 4* A series of photographs showing crack propagation in the polymer containing 10% of particles (strain rate = $12\,sec^{-1}$): (a) 2, (b) 3, (c) 5, (d) 7, (e) 9, (f) 10, (g) 14, (h) 18 $\mu$sec.

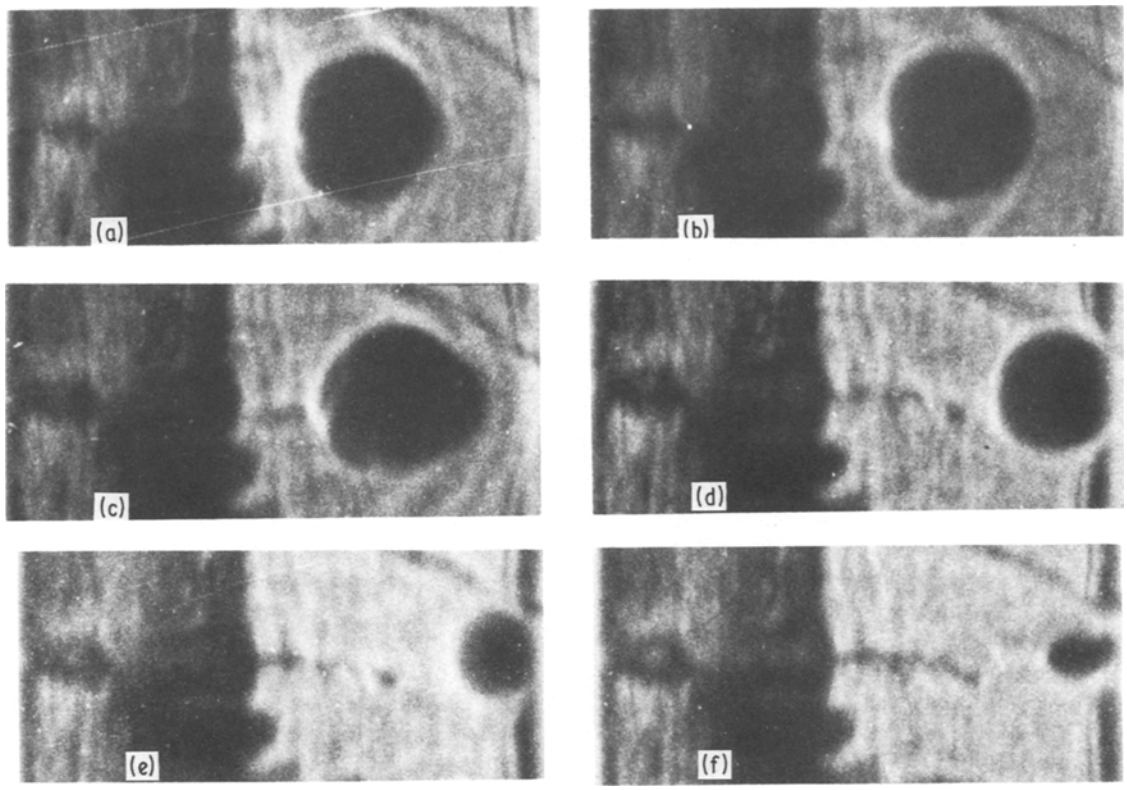


*Figure 5* A series of photographs showing crack propagation in the polymer containing 20% of particles (strain rate = $12\,sec^{-1}$): (a) 6, (b) 7, (c) 8, (d) 13, (e) 15, (f) 19 $\mu$sec.

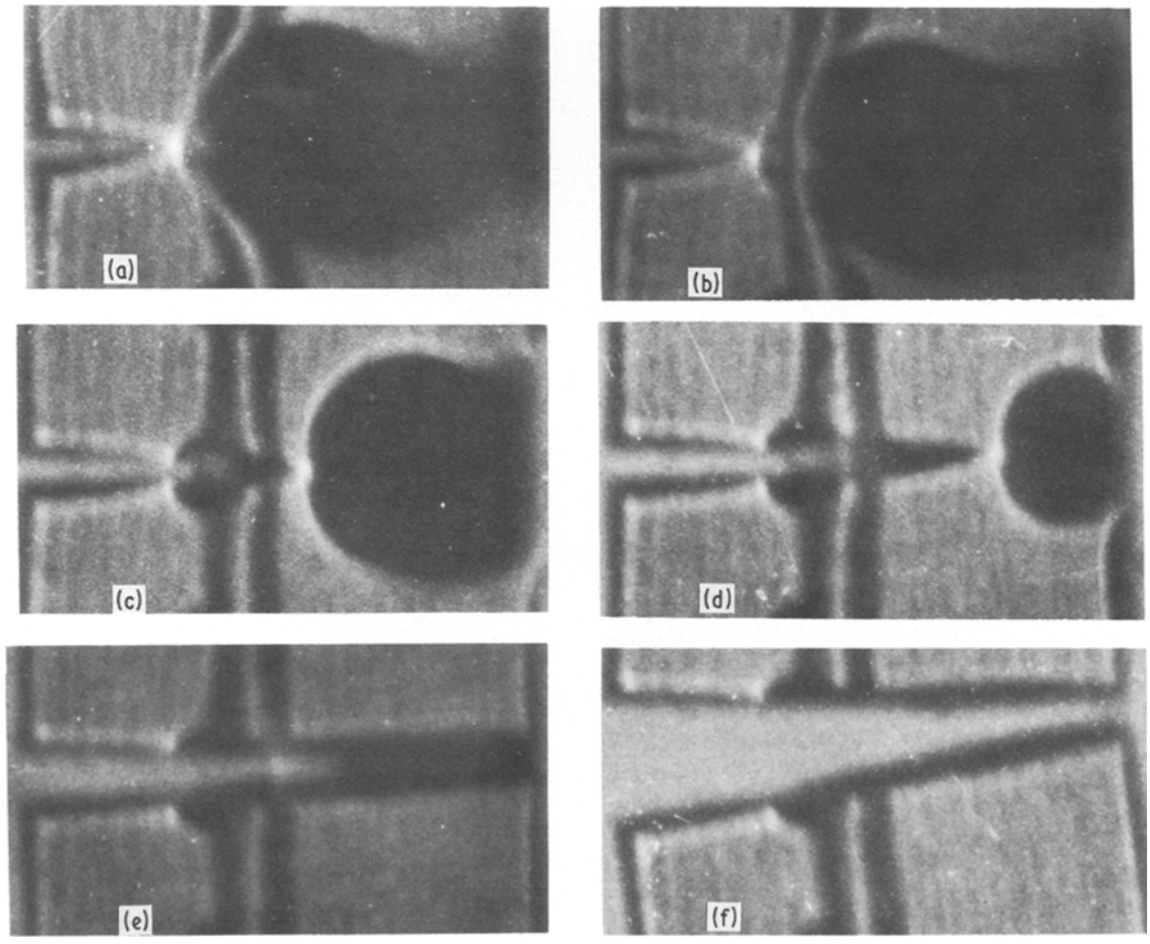


*Figure 6* A series of photographs showing crack propagation in the polymer containing 40% of particles (strain rate = $12\,sec^{-1}$): (a) 5, (b) 17, (c) 81, (d) 113, (e) 177, (f) 497 $\mu$sec.

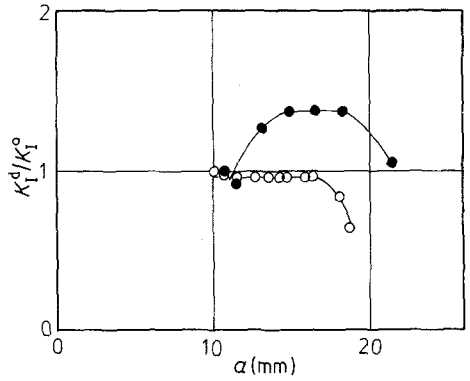


*Figure 7* Variation of $K_I^d/K_I^0$ with crack length for pure PMMA: (●) strain rate $\simeq 4\,sec^{-1}$, (○) strain rate $= 12\,sec^{-1}$.

place immediately the circuit is triggered and the size of the caustic (and hence $K_I^d$) remains approximately constant. For the toughened grades of polymer, propagation only occurs after a delay which increases as $K_I^0$ increases. Once propagation takes place the crack grows very rapidly, probably with considerable excess energy, and $K_I^d$ decreases with crack length (and time). This behaviour is interpreted in relation to crack tip blunting in the next section.

### 5.4. Toughening mechanisms

Fig. 10 shows the dependence of $K_I^0$ upon the volume fraction of particles, $V_p$, for two different testing rates. It can be seen that there is a continuous increase in the values of $K_I^0$ as the amount of particles in the polymer increases. This is consistent with the improvement in impact properties which is found with such systems on the addition of the particles [20]. The dependence of $K_I^0$ upon testing rate gives a useful insight into the toughening processes involved. It can be seen from Fig. 10 that for the pure PMMA $K_I^0$ increases with increasing rate, whereas it decreases with rate for the composites.

The behaviour of the pure PMMA is consistent with previous observations on high-speed crack propagation, where above crack velocities of the order of $1\,m\,sec^{-1}$ the value of the stress intensity factor increases with increasing rate and velocity [1]. Initial crack velocities of the order of $200\,m\,sec^{-1}$ were measured for the PMMA samples.

In the case of the rubber-modified composite samples an increase in testing rate leads to a reduction in the value of $K_I^0$, but with $K_I^0$ always being higher than that for the pure PMMA. This behaviour is consistent with the toughening taking place through crack tip blunting [1]. Previous studies [5] have shown that the relatively small volume increases measured during the plastic deformation in rubber-toughened PMMA imply that the main deformation process induced by the presence of rubber particles is shear yielding, rather than crazing which is found in polymers such as high-impact polystyrene [4]. Increasing the rate of deformation will cause an increase in the shear yield stress of the rubber-toughened polymer. This leads to a sharper crack and a lower value of $K_I^0$ at higher testing rates.

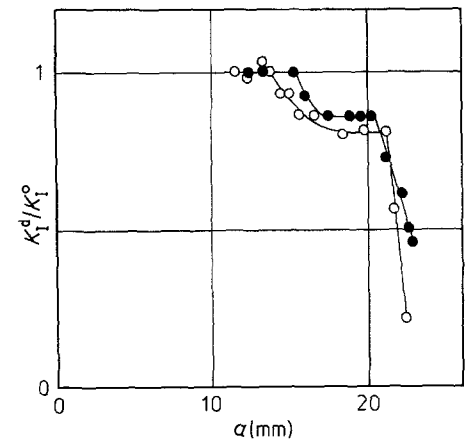


*Figure 8* Variation of $K_I^d/K_I^0$ with crack length for PMMA with 10% of particles (symbols have same meaning as in Fig. 7).

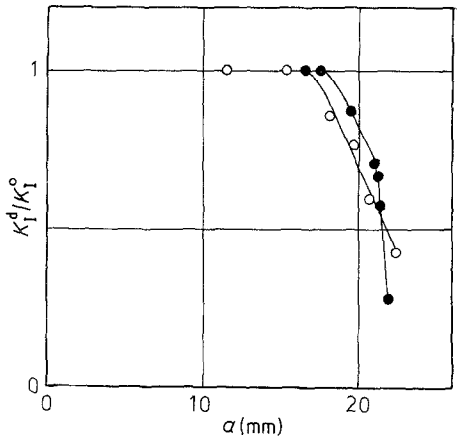


*Figure 9* Variation of $K_I^d/K_I^0$ with crack length for PMMA with 20% of particles (symbols have same meaning as in Fig. 7).

The propagation behaviour of the composite samples is also consistent with toughening taking place through blunting. In each case, the size of the caustic and hence the value of $K_I^d$ decreases with increasing crack length (Figs 4 to 6). Local plastic deformation occurs during the delay period and propagation takes place by the crack bursting through the plastic zone with excess energy. In the case of the 40% volume fraction polymer (Fig. 6) high levels of toughening are obtained through gross plastic deformation taking place at the crack tip, making the linear elastic fracture mechanics analysis not strictly valid.

## 6. Conclusions

It has been shown that the optical method of transmitted caustics can be used to follow the increases in toughness which are found on the addition of second-

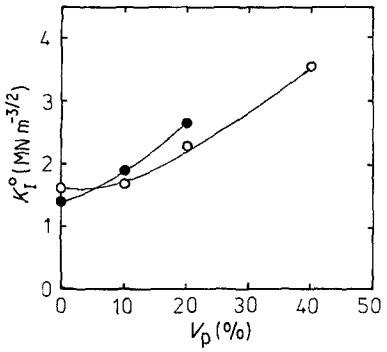


*Figure 10* Dependence of $K_I^0$ upon $V_p$ for toughened PMMA (symbols have same meaning as in Fig. 7).

phase rubber particles to a poly (methyl methacrylate) matrix, because these particulate composites retain good transparency. It has been found that there is a continuous increase in the initiation value of the dynamic stress intensity factor as the volume fraction of particles increases. The indications are that the principal toughening mechanisms is shear yielding which causes crack tip blunting in the composites.

## Acknowledgements

The authors are grateful to Rohm and Haas (UK) Ltd for supplying the polymer samples, to Y. Mahgerefteh for help with the electron microscopy, and to Messrs. K. Sfetsios and A. Kontsambessis for help in crack-propagation experiments.

## References

1. A. J. KINLOCH and R. J. YOUNG, "Fracture Behaviour of Polymers" (Applied Science, London, 1983).
2. P. S. THEOCARIS, G. C. PAPANICOLAOU and E. A. KONTOU, *Reinf. Plast. Compos.* **1** (1982) 206.
3. J. SPANOUDAKIS and R. J. YOUNG, *J. Mater. Sci.* **19** (1984) 473.
4. C. B. BUCKNALL, "Toughened Plastics" (Applied Science, London, 1977).
5. C. B. BUCKNALL, I. K. PARTRIDGE and M. V. WARD, *J. Mater. Sci.* **19** (1984) 2064.
6. W. G. KNAUSS and H. K. MUELLER, in Proceedings of 1st USA–USSR Symposium on Fracture of Composite Materials, September 1978, edited by G. C. Sih and V. P. Tanuzs.
7. P. S. THEOCARIS, G. C. PAPANICOLAOU and G. A. PAPADOPOULOS, *J. Compos. Mater.* **15** (1981) 41.
8. D. MAXWELL, R. J. YOUNG and A. J. KINLOCH, *J. Mater. Sci. Lett.* **3** (1984) 9.
9. J. SPANOUDAKIS and R. J. YOUNG, *J. Mater. Sci.* **19** (1984) 487.
10. C. J. HOOLEY, D. R. MOORE, M. WHALE and M. J. WILLIAMS, *Plast. Rubb. Process. Appl.* **1** (1981) 345.
11. P. MANOGG, *Glastechn. Ber.* **39** (1966) 323.
12. T. KOBAYASHI and J. W. DALLY, ASTM STP 627 (American Society for Testing and Materials, Philadelphia, 1977) p. 257.
13. J. F. KALTHOFF, J. BEINERT and S. WINKLER, ASTM STP 627 (American Society for Testing and Materials, Philadelphia, 1977) p. 161.
14. P. S. THEOCARIS and G. A. PAPADOPOULOS, *Eng. Fract. Mech.* **13** (1980) 683.
15. P. S. THEOCARIS and J. MILIOS, *ibid.* **13** (1979) 599.
16. *Idem, Int. J. Fract.* **16** (1980) 31.
17. P. S. THEOCARIS and J. PRASSIONAKIS, *J. Appl. Polm. Sci.* **22** (1978) 1725.
18. P. S. THEOCARIS and J. MILIOS, *Int. J. Solid Struct.* **17** (1981) 217.
19. *Idem, J. Reinf. Plast. Compos.* **2** (1983) 18.
20. Rohm and Haas Ltd, UK Patent 1 340 025 (1983).

*Received 20 January*
*and accepted 14 March 1986*